

# Curvature-coupling dependence of membrane protein diffusion coefficients

Stefan M. Leitenberger, Ellen Reister-Gottfried, and Udo Seifert

*II. Institut für Theoretische Physik, Universität Stuttgart, 70550 Stuttgart, Germany*

October 26, 2018

## Abstract

We consider the lateral diffusion of a protein interacting with the curvature of the membrane. The interaction energy is minimized if the particle is at a membrane position with a certain curvature that agrees with the spontaneous curvature of the particle. We employ stochastic simulations that take into account both the thermal fluctuations of the membrane and the diffusive behavior of the particle. In this study we neglect the influence of the particle on the membrane dynamics, thus the membrane dynamics agrees with that of a freely fluctuating membrane. Overall, we find that this curvature-coupling substantially enhances the diffusion coefficient. We compare the ratio of the projected or measured diffusion coefficient and the free intramembrane diffusion coefficient, which is a parameter of the simulations, with analytical results that rely on several approximations. We find that the simulations always lead to a somewhat smaller diffusion coefficient than our analytical approach. A detailed study of the correlations of the forces acting on the particle indicates that the diffusing inclusion tries to follow favorable positions on the membrane, such that forces along the trajectory are on average smaller than they would be for random particle positions.

## 1 Introduction

During the last decade it has become more and more apparent that lateral diffusion of proteins in membranes plays a crucial role in cellular functioning.<sup>1,2</sup> Therefore, a whole range of experimental techniques has been developed, which is constantly being improved in order to determine accurate values of lateral protein diffusion coefficients.<sup>3,4</sup> The most important methods include fluorescence recovery after photo bleaching,<sup>5,6</sup> fluorescence correlation spectroscopy,<sup>7,8</sup> or single particle tracking.<sup>9,10</sup> While a large amount of data has been collected with these techniques the interpretation of results always depends on reliable models for the diffusive process. In some situations, like restricted diffusion due to corrals,<sup>10–12</sup> a certain, often rather crude, qualitative explanation is easily found, in other situations, however, this is by no means the case and a reliable quantitative interpretation can only be achieved, if corresponding theoretical calculations or simulations are performed.

Only recently an increased interest in lateral diffusion has emerged from a theoretical viewpoint. In order to compare theoretical results with experiments it is necessary to take into account various aspects of the particular system. These include the nature of the membrane the particle is diffusing in, the properties of the diffusing particle, or the experimental method with which diffusion coefficients are determined. A very important aspect in both theoretical calculations and the analysis of experimental results is that the membrane must not be regarded as a flat plane but is often structured such that regions with higher and lower curvatures appear. For example, this must be accounted for in the study of diffusion in the membranes of the endoplasmic reticulum. Neglecting the influence of the membrane shape leads to considerable errors in the determination of diffusion coefficients.<sup>13</sup> Several analytical and simulational studies have been performed that regard diffusion on various fixed curved surfaces.<sup>14–20</sup>

But even if a membrane appears to be flat on average, it is subject to thermal fluctuations that lead to rapid shape changes around the flat configuration.<sup>21,22</sup> Neglecting the influence of the membrane on the movement of the particle these fluctuations that depend on properties

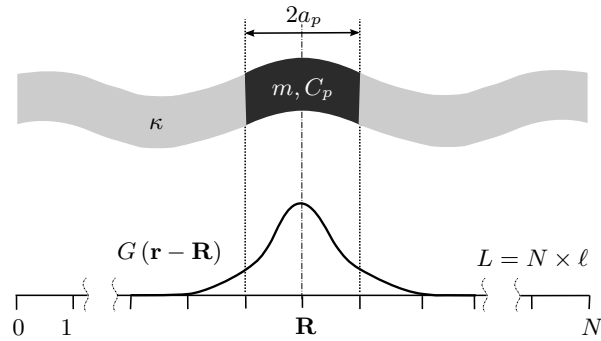


Figure 1: Sketch of the curvature-coupled model for an inclusion at position  $\mathbf{R}$ , with area  $\pi a_p^2$ , a bending rigidity  $m$  and a spontaneous curvature  $C_p$  in a model membrane with the bending rigidity  $\kappa$  and the effective surface tension  $\sigma$ . The membrane is mapped to a two-dimensional  $N \times N$  lattice with the lattice spacing  $\ell$  of which only a one-dimensional cut is shown here. The lateral dimension of the system is  $L = N \times \ell$ . In the simulations, the area of the inclusion is determined by the weighting function  $G(\mathbf{r} - \mathbf{R})$ , which is set to be a Gaussian.

like bending rigidity, surface tension, proximity to substrates or other membranes, etc., have an influence on the measured values for lateral diffusion coefficients because experiments usually regard the path of the inclusion projected on a flat reference plane instead of the actual path along the membrane. Compared to the intramembrane diffusion coefficient the measured diffusion coefficient will be the smaller the stronger the fluctuations. This was initially pointed out by Gustafsson and Halle;<sup>23</sup> the quantitative evaluation of this effect for free intramembrane diffusion was performed more recently in independent work by us and two other groups using analytical calculations<sup>24,25</sup> and simulations.<sup>20,26</sup>

All studies mentioned in the last two paragraphs take into account the influence of the shape of the membrane on measured diffusion coefficients, but otherwise neglect any interaction between membrane and protein. Considering that a protein also has certain physical properties it must be assumed that interactions between the protein and the membrane exist that influence the diffusion coefficient. This assumption is corroborated by experimental findings: for example after photoactivation of bacteriorhodopsin (BR) in model membranes the lateral diffusion coefficient is reduced by a factor of five.<sup>27</sup> This reduction is attributed to oligomerization of BR upon activation caused by structural changes that influence protein-lipid interactions. There are many other experimental examples that indicate that the interactions between membrane and protein have a significant influence on lateral diffusion, see for example refs.<sup>28,29</sup> An important property of a membrane compared to a flat surface is the curvature. A variety of studies mainly using particle based simulations are concerned with the influence of inclusions with a certain intrinsic curvature on membrane shape and lateral diffusion.<sup>30–38</sup> In earlier work we calculated effective diffusion coefficients for particles with a bending rigidity and a spontaneous curvature.<sup>24</sup> These calculations revealed that the additional interaction that tries to move the particle to positions on the membrane where the curvature agrees with the particle's spontaneous curvature, leads to an increase in the diffusion coefficient.

Our previous work on curvature-coupled diffusion effectively describes diffusion of a point-like particle and relies on several approximations.<sup>24,26</sup> One of these, the so-called pre-averaging approximation, assumes that membrane fluctuations on all possible length scales have a much shorter relaxation time than the time it takes the particle to diffuse the corresponding distance. In this paper we introduce a scheme to simulate the diffusion of a particle with a certain extension, a bending rigidity and a spontaneous curvature in a thermally fluctuating membrane. A sketch of the considered system with the relevant physical parameters is given in fig. 1.

The present method is no longer restricted to certain relative timescales of diffusion and membrane fluctuations. The additional energy of the inclusion is introduced by replacing a patch of membrane that is described by the Helfrich Hamiltonian with a new Helfrich-like term with a different bending rigidity and a spontaneous curvature. The extension of the particle is modeled by a Gaussian weighting function in order to have a smooth crossover from the bare membrane to

the particle. Obviously the system is dominated by two dynamic processes: the shape fluctuations of the membrane and the particle diffusion. Two Langevin-equations, one for the membrane, the other for the particle, are derived from the energy of the system. Our simulation scheme consists of the numerical integration in time of these coupled equations. Apart from performing simulations we also analytically evaluate the coupled dynamic equations by use of a perturbation theory that neglects the influence of the particle on the membrane and assumes that membrane relaxation times are much smaller than corresponding diffusive time scales. In order to compare with these analytical calculations and to reduce the computational effort, we restrict our simulations in the current study such that the membrane dynamics is also not influenced by the diffusing particle. The influence on membrane movement will be considered in future work. The main quantity of interest is the ratio of the curvature-coupled and the intramembrane diffusion coefficient as a function of the membrane parameters bending rigidity and surface tension. The latter coefficient is a parameter of our scheme and resembles the free diffusion coefficient of the particle if no additional force were acting on it. The application of both our approaches shows that curvature-coupling leads to increased diffusion. However, the comparison of our analytic calculations with the simulation results reveals a systematic difference. In order to gain insight into the reason for these discrepancies we study force correlation functions that are the main contributions to the diffusion constant.

The paper is organized as follows: In the following section we explain the model for the membrane dynamics and the Langevin-equation for the inclusion. In sec. 3, the method and the approximations of the analytical calculation of the curvature-coupled diffusion coefficient are presented while sec. 4 introduces the used simulation scheme. Sec. 5 discusses the choice of parameters used in both the calculations and the simulations. The presentation of the results in sec. 6 is followed by a detailed discussion in sec. 7, why simulations lead to smaller diffusion constants and a possible interpretation of our findings. The paper finishes with some conclusions and an outlook for future work.

## 2 Model

### 2.1 Membrane dynamics

We consider a model membrane in a fluid environment. The membrane is given in Monge-representation where  $\mathbf{r} \equiv (x, y)^T$  is the position in the  $(x, y)$ -plane with the deviation  $h(\mathbf{r}, t)$  out of this plane. For such a membrane Helfrich<sup>39</sup> derived the free energy that to lowest order has the following form in the Monge-gauge<sup>40</sup>

$$\mathcal{H}_0[h(\mathbf{r}, t)] = \int_{L^2} d\mathbf{r} \left[ \frac{\kappa}{2} (\nabla_{\mathbf{r}}^2 h(\mathbf{r}, t))^2 + \frac{\sigma}{2} (\nabla_{\mathbf{r}} h(\mathbf{r}, t))^2 \right], \quad (1)$$

with the bending rigidity  $\kappa$ , the effective surface tension  $\sigma$  and the area  $L^2$  in the  $(x, y)$ -plane. The dynamics of a membrane is given by<sup>22</sup>

$$\partial_t h(\mathbf{r}, t) = - \int_{L^2} d\mathbf{r}' \Lambda(\mathbf{r} - \mathbf{r}') \frac{\delta \mathcal{H}_0}{\delta h(\mathbf{r}', t)} + \xi(\mathbf{r}, t) \quad (2)$$

with the Onsager coefficient  $\Lambda(\mathbf{r} - \mathbf{r}')$  that takes into account hydrodynamic interactions with the fluid background. Using the Fourier-transformation

$$h(\mathbf{k}, t) = \int_{L^2} d\mathbf{r} h(\mathbf{r}, t) \exp \{-i\mathbf{r} \cdot \mathbf{k}\} \quad (3)$$

$$h(\mathbf{r}, t) = \frac{1}{L^2} \sum_{\mathbf{k}} h(\mathbf{k}, t) \exp \{i\mathbf{r} \cdot \mathbf{k}\} \quad (4)$$

one obtains (2) in Fourier-space

$$\partial_t h(\mathbf{k}, t) = -\Lambda(k)E(k)h(\mathbf{k}, t) + \xi(\mathbf{k}, t) \quad (5)$$

with  $E(k) \equiv \kappa k^4 + \sigma k^2$  and  $\Lambda(k) \equiv 1/(4\eta k)$  which is the Fourier-transformed Onsager coefficient for a free membrane in a fluid with viscosity  $\eta$ .<sup>22</sup> The stochastic force  $\xi(\mathbf{k}, t)$  obeys the fluctuation-dissipation theorem

$$\langle \xi(\mathbf{k}, t) \rangle = 0, \quad (6)$$

$$\langle \xi(\mathbf{k}, t) \xi^*(\mathbf{k}', t') \rangle = 2\Lambda(k) \frac{L^2}{\beta} \delta(t - t') \delta_{\mathbf{k}, \mathbf{k}'}, \quad (7)$$

where  $\beta \equiv (k_b T)^{-1}$  is the inverse temperature. Later on, we need the correlations of  $h(\mathbf{k}, t)$  which are given by

$$\langle h(\mathbf{k}, t) \rangle = 0, \quad (8)$$

$$\langle h(\mathbf{k}, t) h^*(\mathbf{k}', t') \rangle = \frac{L^2}{\beta E(k)} \exp[-\Lambda(k) E(k) |t - t'|] \delta_{\mathbf{k}, \mathbf{k}'}. \quad (9)$$

## 2.2 Diffusion

Now we place an inclusion into the membrane that diffuses freely along the membrane. The dynamics of the inclusion may be described by a Fokker-Planck-equation (FP-eq.). However, since the diffusive motion takes place on a curved surface the Laplace-operator needs to be replaced by the Laplace-Beltrami-operator. This leads to a new FP-eq.<sup>24,26</sup>

$$\partial_t P(\mathbf{r}, t) = D \sum_{i,j} \partial_i \sqrt{g} g^{ij} \partial_j \frac{1}{\sqrt{g}} P(\mathbf{r}, t), \quad (10)$$

with the diffusion coefficient  $D$ , the metric  $g$  and the inverse metric tensor  $g^{ij}$ . In the Monge gauge the metric has the form  $g \equiv 1 + h_x^2 + h_y^2$ , while the inverse metric tensor is

$$g^{ij} \equiv \begin{pmatrix} 1 + h_y^2 & -h_x h_y \\ -h_x h_y & 1 + h_x^2 \end{pmatrix}. \quad (11)$$

The subscripts denote partial derivatives, e.g.  $h_x \equiv \partial h / \partial x$ . The probability  $P(\mathbf{r}, t)$  of finding the projection of the inclusion at a position  $\mathbf{r}$  is normalized to  $\int d\mathbf{r} P(\mathbf{r}, t) = 1$ . In the simulations we make use of a Langevin-equation to describe the motion of the projected particle position  $\mathbf{R}(t) = (X(t), Y(t))^T$ . Using the above FP-eq. a projected Langevin-eq. is derived within the Stratonovich calculus:<sup>41,42</sup>

$$\begin{aligned} \partial_t X(t) &= D \frac{1}{g(\sqrt{g} + 1)} (h_Y h_{XY} - h_X h_{YY}) \\ &\quad + \sqrt{D} \frac{1}{g - 1} \left[ \left( \frac{h_X^2}{\sqrt{g}} + h_Y^2 \right) \zeta_X(t) + \right. \\ &\quad \left. h_X h_Y \left( \frac{1}{\sqrt{g}} - 1 \right) \zeta_Y(t) \right], \\ \partial_t Y(t) &= D \frac{1}{g(\sqrt{g} + 1)} (h_X h_{XY} - h_Y h_{XX}) \\ &\quad + \sqrt{D} \frac{1}{g - 1} \left[ h_X h_Y \left( \frac{1}{\sqrt{g}} - 1 \right) \zeta_X(t) + \right. \\ &\quad \left. \left( \frac{h_Y^2}{\sqrt{g}} + h_X^2 \right) \zeta_Y(t) \right]. \end{aligned} \quad (12)$$

The upper case subscripts express that the partial derivatives at the particle position  $\mathbf{R}(t)$  have to be used. The stochastic force  $\zeta$  has zero mean and is delta-correlated:

$$\langle \zeta_i \rangle = 0, \quad (13)$$

$$\langle \zeta_i(t) \zeta_j(t') \rangle = 2\delta_{ij} \delta(t - t'). \quad (14)$$

Equation (12) comprises a drift that is caused by the membrane curvature and diffusive terms. The consequences of such a drift term for a freely diffusing inclusion have been introduced in ref.<sup>26</sup>

## 2.3 Curvature-coupled model

The equations derived so far apply to a freely diffusing point-like inclusion. If one is interested in the diffusion of a more realistic inclusion, one has to take the physical parameters of the inclusion into account. First the inclusion has a non vanishing area which is set to  $\pi a_p^2$ . Furthermore, the inclusion has possibly its own bending rigidity  $m$  and maybe a spontaneous curvature  $C_p$ . As indicated by “into the membrane” the inclusion completely replaces the membrane at its position. To consider this in the free energy of the system, one has to add a new energy term for the inclusion and remove the part of the membrane which is replaced. The additional term caused by the inclusion leads to the new free energy

$$\mathcal{H} = \mathcal{H}_0 + \mathcal{H}_1, \quad (15)$$

where

$$\mathcal{H}_1[h(\mathbf{r}, t), \mathbf{R}(t)] = \int_{L^2} d\mathbf{r} G(\mathbf{r} - \mathbf{R}) \times \left[ \frac{m}{2} (\nabla_{\mathbf{r}}^2 h(\mathbf{r}, t) - C_p)^2 - \frac{\kappa}{2} (\nabla_{\mathbf{r}}^2 h(\mathbf{r}, t))^2 \right] \quad (16)$$

is the correction to Helfrich’s free energy  $\mathcal{H}_0$ .  $G(\mathbf{r} - \mathbf{R})$  is a weighting function for the extension of the particle that we set to be a Gaussian such that the crossover from particle to membrane is smooth. Taking into account the area constraint  $\int d\mathbf{r} G(\mathbf{r} - \mathbf{R}) = \pi a_p^2$  it is given by

$$G(\mathbf{r} - \mathbf{R}) = \exp \left\{ -\frac{(\mathbf{r} - \mathbf{R})^2}{a_p^2} \right\}. \quad (17)$$

The altered free energy (16) induces additional forces on the inclusion and the membrane. The membrane dynamics is obtained by replacing  $\mathcal{H}_0$  in (2) with  $\mathcal{H}$  such that

$$\partial_t h(\mathbf{r}, t) = - \int_{L^2} d\mathbf{r}' \Lambda(\mathbf{r} - \mathbf{r}') \left( \frac{\delta \mathcal{H}_0}{\delta h(\mathbf{r}', t)} + \frac{\delta \mathcal{H}_1}{\delta h(\mathbf{r}', t)} \right) + \xi(\mathbf{r}, t). \quad (18)$$

The forces that influence the diffusive behavior of the inclusion can be calculated by  $\mathbf{f} \equiv -\nabla_{\mathbf{R}} \mathcal{H}_1$ . Taking into account the curvature of the membrane in the force term, which needs to be added to the right hand side of (12), we get the complete equation of motion for the inclusion

$$\partial_t \mathbf{R}_i(t) = \partial_t \mathbf{R}_{proj,i} - \mu \frac{1}{g} \sum_j g^{ij} \partial_j \mathcal{H}_1, \quad (19)$$

with the mobility  $\mu$  that is related to the intramembrane diffusion coefficient  $D$  via the Einstein relation  $D = k_b T \mu$ .

With eqs. (18) and (19) the dynamics of the system is fully determined. Note, that these equations are coupled since the particle diffusion depends on the shape of the membrane via the partial derivatives of  $h(\mathbf{r}, t)$  at the particle position, and the membrane dynamics on the position of the particle through the additional energy.

## 3 Analytical calculations

In order to calculate a new curvature-coupling affected diffusion coefficient defined as

$$D_{cc} \equiv \lim_{t \rightarrow \infty} \frac{\langle \Delta \mathbf{R}^2(t) \rangle}{4t}, \quad (20)$$

one has to determine the mean square displacement

$$\langle \Delta \mathbf{R}^2(t) \rangle \equiv \int_0^t d\tau \int_0^t d\tau' \langle \partial_{\tau} \mathbf{R}(\tau) \cdot \partial_{\tau'} \mathbf{R}(\tau') \rangle, \quad (21)$$

by integrating eq. (19) in time and performing the thermal average. Since the explicit calculation of the mean square displacement using the exact equation of motion (19) and the full membrane dynamics (18) is not possible analytically, it is necessary to introduce several approximations.

In order to simplify eq. (19) we perform a pre-averaging approximation. This approximation is applicable if for all modes the membrane relaxation times  $(\Lambda(k)E(k))^{-1}$ , see eq. (9), are considerably shorter than the time  $\pi^2/(Dk^2)$  it takes a particle to diffuse the distance given by the corresponding wave length of the mode. For typical experimental values for bending rigidity  $\kappa$ , tension  $\sigma$ , diffusion coefficients  $D$ , and system sizes  $L$ , this condition is very often fulfilled. If membrane fluctuations are “faster” than the diffusion of the particle it is assumed that the particle only feels average membrane fluctuations. The applicability of this approximation for free lateral diffusion is discussed in ref.<sup>26</sup> In our current work the pre-averaging approximation results in the replacement of  $\mu \frac{1}{g} g^{ij}$  in eq. (19) by  $\mu_{proj} \delta_{ij}$  where the projected free mobility is defined by  $\mu_{proj} \equiv \mu(1 + \langle 1/g \rangle)/2$ .<sup>24,26</sup>

We, furthermore, assume that the additional energy  $\mathcal{H}_1$  caused by the insertion of a single particle is small, in order to justify a perturbation expansion to first order in the particle energy. The consequence of this approximation is that the dynamics of the membrane is not influenced by the presence of the inclusion. Thus the membrane dynamics is expressed by eq. (5).

Another approximation needs to be employed so as to make analytical calculations possible. Inserting eq. (19) into eq. (21) we see that the mean square displacement becomes a function of the height correlations  $\langle h(\mathbf{R}(t), t) h(\mathbf{R}(t'), t') \rangle$ . These correlations decay with increasing time difference  $|t - t'|$  due to two reasons: during the time interval the membrane shape changes and the particle position advances. Since we assume diffusion to be much slower than membrane shape changes we neglect the effect caused by the particle movement.

Note, that this approximative analytical calculation cannot include a possible correlation between the particle position and the membrane shape in the vicinity of the inclusion. In other words, we assume a constant probability for finding the particle at any point in the system relative to a given membrane configuration. This aspect becomes important when we compare with simulation results, as will be discussed in sec. 7.

Using the inverse Fourier-transform given in eq. (4) and applying the previously explained approximations we find for the mean square displacement

$$\begin{aligned} \langle \Delta \mathbf{R}^2(t) \rangle &= 4D_{proj}t + \\ &+ m^2 C_p^2 \mu_{proj}^2 \int_0^t d\tau \int_0^t d\tau' \frac{1}{L^4} \sum_{\mathbf{k}} \sum_{\mathbf{k}'} (\pi a_p^2)^2 k^2 k'^2 \mathbf{k} \cdot \mathbf{k}' \times \\ &\times \exp \left\{ -i\mathbf{R} \cdot (\mathbf{k} + \mathbf{k}') - \frac{(k^2 + k'^2) a_p^2}{4} \right\} \langle h(\mathbf{k}, t) h(\mathbf{k}', t') \rangle \end{aligned} \quad (22)$$

with the height correlation function given in eq. (9) and  $D_{proj} = k_b T \mu_{proj}$ .

Inserting the resulting equation for  $\langle \Delta \mathbf{R}^2(t) \rangle$  into (20) and performing the long time limit one gets

$$\begin{aligned} D_{cc} &= D_{proj} + \mu_{proj}^2 m^2 C_p^2 (\pi a_p^2)^2 \frac{1}{L^2} \times \\ &\times \sum_{\mathbf{k}} k^6 \exp \left\{ -\frac{k^2 a_p^2}{2} \right\} \frac{1}{2\beta E^2(k) \Lambda(k)}. \end{aligned} \quad (23)$$

In this equation it is interesting that there is no need to set a cut-off for the wavenumber  $\mathbf{k}$  since the exponential function  $\exp \{-k^2 a_p^2/2\}$  damps higher  $\mathbf{k}$  values. In ref.<sup>24</sup> a similar calculation for the curvature coupled diffusion coefficient is performed. There the area function has the form  $\pi a_p^2 \delta(\mathbf{r} - \mathbf{R})$  and a cut-off is necessary. The resulting diffusion coefficient agrees with the above diffusion coefficient of equation (23) in the limit of vanishing variance of the Gaussian.

## 4 Simulation method

To probe the applicability of our analytical calculations that depend on several approximations we set up simulations that numerically integrate the coupled equations of motion for the membrane and the diffusing particle. We use a square, periodic lattice with  $N \times N$  lattice points and the lattice spacing  $\ell$  to map a model membrane with size  $L = N \times \ell$ , see fig 1. To simulate the shape fluctuations of the membrane we numerically integrate the appropriate equation of motion. In order to reduce the computational effort and to compare with the analytical calculations introduced in the previous section we evaluate the unperturbed Langevin-equation (5) discretely in time. These calculations are performed in Fourier-space since the equations of motion for the height function modes  $h(\mathbf{k}, t)$  decouple. Due to the periodic boundary conditions the wave vectors are of the form  $\mathbf{k} = 2\pi(l, n)/L$  with  $l$  and  $n$  being integers. Since the height function  $h(\mathbf{r})$  is a real function defined on a  $N \times N$  lattice the relation  $h(\mathbf{k}, t) = h^*(-\mathbf{k}, t)$  applies leading to the restriction  $-N/2 < l, n \leq N/2$ .

Regarding the fluctuation-dissipation theorem (7) it is obvious that fluctuations of  $h(\mathbf{k} = 0, t)$  would diverge for the Onsager-coefficient  $\Lambda(\mathbf{k} \rightarrow 0) \rightarrow \infty$ . The dynamics of the height function mode  $h(\mathbf{k} = 0, t)$  corresponds to the center of mass movement of the whole membrane. Due to the irrelevance of this movement in the determination of the lateral diffusion coefficient we set  $\Lambda(\mathbf{k} = 0) = 0$  and keep  $h(\mathbf{k} = 0, t) = 0$  fixed at all times.

In order to choose an appropriate discrete time step  $\Delta t$  that ensures that numerical errors are small it is necessary to point out that the largest  $\mathbf{k}$ -vector possible  $k_{max} = \sqrt{2}\pi N/L$  in the given lattice determines the smallest time scale of the membrane as can be seen in eq. (9). The used time step  $\Delta t$  in the simulation should be smaller than this smallest time scale.

The dynamics of the inclusion is given by a discrete version of eq. (19) that is also numerically integrated in time. Since it is coupled to the membrane equation (5) via the derivatives  $h_X, h_Y$ , etc., of the membrane configuration at the position of the inclusion, the temporal evolution during a discrete time step  $\Delta t$  consists of an update of the membrane shape and the particle position. In contrast to the membrane dynamics the motion of the inclusion is calculated in real space. The required derivatives of  $h(\mathbf{r}, t)$  are, therefore, determined in Fourier-space and then transformed to real space using routines of the FFTW-libraries.<sup>43</sup> We allow off-lattice diffusion for the inclusion which is necessary if the average time it takes a particle to diffuse a distance  $\ell$  is much larger than the corresponding membrane relaxation time. Thus the derivatives at the position of the inclusion are determined by a distance weighted linear extrapolation of the four nearest lattice sites. In order to minimize the numerical error caused by not following the membrane surface correctly the displacement per time step is to be set to a small fraction of the lattice spacing  $\ell$ . With the above explained restriction for the time step in order to describe the membrane shape evolution with sufficient accuracy there are overall two conditions that must be fulfilled in the choice of  $\Delta t$ .

Apart from obvious computational limits the determination of how long simulation runs should at least be is again dictated by two time scales. On the one hand the length of the simulation should be several times the longest relaxation time of the membrane, which is given by the smallest possible wave vector, to ensure that the membrane shape has passed through an adequate amount of independent configurations. On the other hand it is preferable that the inclusion has enough time on average to cover a distance of several lattice sites.

A more detailed description of the simulation method is given in ref.,<sup>26</sup> where the corresponding scheme for free particle diffusion has been introduced.

## 5 Parameters

Before we present our results we will introduce the used parameters. These are the same for the analytical calculations and the simulations. As already mentioned in the description of the simulation method we use a discrete membrane with a lattice spacing of  $\ell$  that we set to  $\ell = 10\text{nm}$ . This choice reflects a compromise between the wish to simulate reasonably sized systems and the computational limitation in the number of lattice sites. A decrease in the lattice spacing for a constant system size, i.e. an increase in the number of lattice sites, introduces additional large  $k$ -values that contribute only weakly to membrane fluctuations, see eq. (9), or the curvature-coupled diffusion coefficient (23).  $\ell$  is one of the basic units. The others are the time given in seconds  $s$



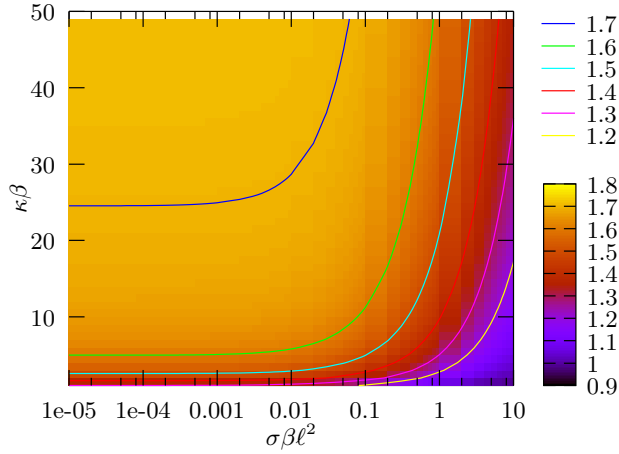


Figure 2: Ratio of the curvature-coupled diffusion coefficient to the free diffusion  $D_{cc}/D$  as a function of the bending rigidity  $\kappa\beta$  and the effective tension  $\sigma\beta\ell^2$ .

and the thermal energy that is  $\beta^{-1} = 4.14 \times 10^{-21} \text{J}$  at room temperature. All parameters of the system are given in units of  $\ell$ ,  $s$ , and  $\beta$ . For the determination of the membrane parameters we look at typical experiments and extract a range of 5 to 50 for the bending rigidity  $\kappa\beta$  and  $10^{-9}$  to  $10^{-6} \text{J/m}^2$  for the effective tension  $\sigma$  that corresponds to  $10^{-5}$  to  $10^{-2}$  for  $\sigma\beta\ell^2$ . At around  $\sigma\beta\ell^2 = 10$  rupture of the membrane occurs. In the experiments it is, furthermore, common to use water as a surrounding medium with a viscosity of  $\eta = 10^{-3} \text{kg/ms} = 2.47 \times 10^{-7} \text{s}/(\beta\ell^3)$ . The last parameter of the membrane is the size  $L$  that is related to the number of lattice points  $N$  in each direction via  $L = N \times \ell$ . Since a sufficient number of wave vectors  $\mathbf{k}$  are considered for a  $50 \times 50$  lattice we use a system size of  $L = 50\ell$  that corresponds to  $0.5 \mu\text{m}$ . For the parameters of the inclusion we choose  $C_p\ell = 2$ ,  $m\beta = 2\kappa\beta$  and  $a_p = 1\ell$  as in our previous calculations.<sup>24</sup> The bare diffusion coefficient  $D$ , however, has to be chosen carefully. Since the analytical calculations rely on a pre-averaging approximation we have to set  $D$  sufficiently small. Therefore, the time scale of the diffusion  $\tau_D = \pi^2 / (Dk_{min}^2)$  must be much longer than the largest membrane time. This time is given by  $\tau_{memb,max} = 4\eta / (\kappa k_{min}^3 + \sigma k_{min})$  with the absolute value of the smallest wave vector  $k_{min} = 2\pi/L$  which corresponds to the longest length  $L$  in the system. The comparison of the two time scales leads to  $D \ll \pi^2 (\kappa k_{min} + \sigma k_{min}^{-1}) / (4\eta) \sim 10^6 \ell^2/s$ . We choose  $D = 5 \times 10^4 \ell^2/s$ . This choice is good for all values of  $\kappa\beta$  and  $\sigma\beta\ell^2$  in the selected range. For the total length of the simulations one has to keep in mind that it has to be several times longer than the time scale of the longest wave vector. The time step  $\Delta t$  however has to be so small that it is smaller than the shortest membrane time  $\tau_{memb,min}$  and that the inclusion diffuses only a short distance. We set the total length to 1ms and  $\Delta t = 10^{-9} \text{s}$  such that each simulation run comprises  $10^6$  time steps. This choice of the time step  $\Delta t$  is applicable for small bending rigidities  $\kappa\beta$ .

Note, that an increase of  $\kappa\beta$  and  $\sigma\beta\ell^2$  leads to smaller time scales  $\tau_{memb}$  of the membrane. In order not to increase computing time we keep  $\Delta t$  fixed for all considered  $\kappa\beta$  and  $\sigma\beta\ell^2$ . This, however, will lead to a slight increase in numerical errors for the modes  $h(\mathbf{k}, t)$  with very large wave vectors in membranes with large  $\kappa\beta$  and  $\sigma\beta\ell^2$ . Since fluctuations of these modes, see eq. (9), are rather small these errors are negligible in the determination of  $D_{cc}$ .

## 6 Results

The analytically derived curvature-coupled diffusion coefficient  $D_{cc}$  is calculated by numerical summation of equation (23) using *Mathematica* for the whole range of parameters given in the previous section. The ratio  $D_{cc}/D$  of the curvature-coupled  $D_{cc}$  and the free intramembrane diffusion coefficient  $D$  is plotted as a function of the bending rigidity  $\kappa\beta$  and the effective surface tension  $\sigma\beta\ell^2$  in fig. 2. The ratio increases for brighter colors. In the figure one can see that for small  $\sigma\beta\ell^2$  the ratio increases very strongly for  $\kappa\beta < 5$ . With a further increase of the bending rigidity  $\kappa\beta$  the ratio reaches a plateau. Here the strengthening of the forces  $\mathbf{f}$  caused by an increasing



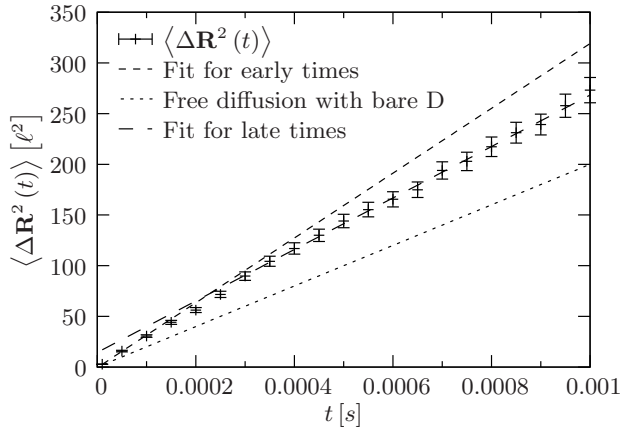


Figure 3: Mean square displacement determined from simulation data as a function of time for  $\kappa\beta = 5$  and  $\sigma\beta\ell^2 = 0$ . Plotted with the data points are the two fits for the diffusion coefficient at the beginning and the end of the simulations. Furthermore, the expected mean square displacement for bare free diffusion is displayed.

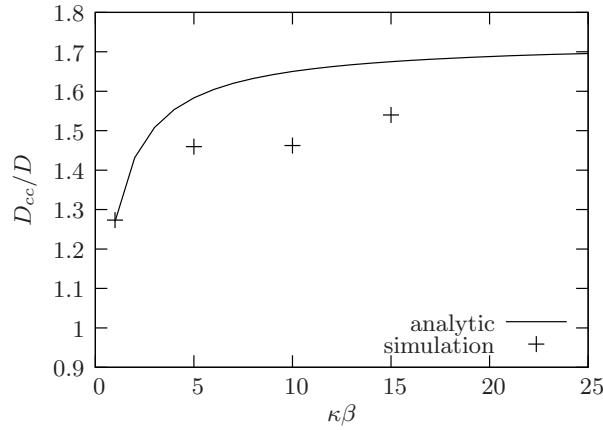


Figure 4: Ratio  $D_{cc}/D$  of the curvature-coupled to the intramembrane diffusion coefficient as a function of bending rigidity  $\kappa\beta$  for fixed surface tension  $\sigma\beta\ell^2 = 1 \times 10^{-2}$ . Most of the simulated data points are smaller than the analytical curve determined by eq. (23).

bending rigidity of the inclusion  $m\beta$  is compensated by the fact that thermal fluctuations become weaker for increasing  $\kappa\beta$ . The increase of  $\sigma\beta\ell^2$  by about three orders of magnitude leads to no significant effect. However, for even larger values of  $\sigma\beta\ell^2$  the ratio decreases fast to one for small  $\kappa\beta$ . This happens since a large surface tension  $\sigma\beta\ell^2$  also damps the thermal fluctuations of the membrane and, therefore, the additional force on the inclusion is small. Increasing  $\kappa\beta$  the ratio also increases for large  $\sigma\beta\ell^2$  but does not reach the same height as for small tensions. In this case the increase of  $D_{cc}/D$  for high values of  $\kappa\beta$  is also compensated by the damping caused by the surface tension.

Overall, our calculations show that the curvature-coupling, which leads to an additional force  $\mathbf{f}$  on the inclusion, enhances the inclusion's diffusion rate in the investigated parameter range. It is noteworthy that the ratio is always bigger than one despite the fact that the projection alone would lead to a ratio smaller than one.<sup>24</sup>

Results from variations of the other parameters, like  $L$ ,  $C_p$ , etc., are not plotted but the effect on  $D_{cc}$  can easily be obtained from eq. (23). However, one has to keep in mind that the effect of the inclusion on the membrane has to be small in order for the perturbation theory to be applicable.

In the simulations, we also use the unperturbed membrane equation of motion (5) and the same parameter sets as for the numerical summation just discussed. As we are interested in results in

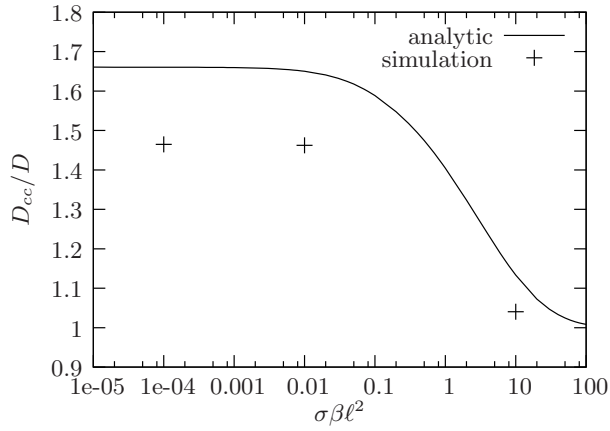


Figure 5: Ratio  $D_{cc}/D$  as a function of  $\sigma\beta\ell^2$  for the fixed bending rigidity  $\kappa\beta = 10$ . The simulated values (+) follow the analytical curve (line) of eq. (23) only qualitatively.

thermal equilibrium each membrane starts in a random configuration and has 1 ms to equilibrate before the inclusion is placed in its center. 1 ms is about five times the longest membrane relaxation time so we can be sure that the membrane is in thermal equilibrium. Since we obtain only one particle trajectory per independent simulation run we average over 500 simulations with the same set of parameters to get the mean square displacement  $\langle\Delta\mathbf{R}^2(t)\rangle$ . An example for  $\langle\Delta\mathbf{R}^2(t)\rangle$  as a function of time is plotted in figure 3. The slope of the resulting straight line at late times corresponds to  $D_{cc}$ , see eq. (20). The determined values for  $D_{cc}/D$  from the simulations (+) are plotted with the analytical curve (line) in fig. 4 as a function of  $\kappa\beta$  for a constant  $\sigma\beta\ell^2$  and in fig. 5 as a function of  $\sigma\beta\ell^2$  for a constant bending rigidity  $\kappa\beta$ . We see that the simulations follow qualitatively the analytical curve but the values are about 10% smaller than expected.

## 7 Discussion

Both of our approaches demonstrate that curvature-coupling enhances diffusion. This result is plausible for the following reason. Due to the membrane fluctuations the positions that are favorable for the diffusing particle are constantly changing. Thus the particle is subject to changing forces leading to enhanced movement of the particle, which in turn leads to a higher diffusion coefficient. The resulting enhanced diffusion coefficient is caused by forces, which are still thermal. Therefore, the system is still in equilibrium and the fluctuation-dissipation-theorem is applicable, such that an increased effective mobility or a reduced effective friction of the particle can be determined.

On the quantitative side, the analysis of the simulation data reveals a diffusion coefficient that is about 10% smaller than we expect from the analytical calculations. In these calculations several approximations that we have explained in sec. 3 are applied to calculate the mean square displacement  $\langle\Delta\mathbf{R}^2(\tau)\rangle$  (21). The dominant contribution to  $D_{cc}$  is  $\langle\mathbf{f}(\tau, \mathbf{R}(\tau)) \cdot \mathbf{f}(\tau + \Delta\tau, \mathbf{R}(\tau + \Delta\tau))\rangle$  with the force  $\mathbf{f}(\tau, \mathbf{R}(\tau)) \equiv -\nabla_{\mathbf{R}}\mathcal{H}_1[h(\mathbf{r}, \tau), \mathbf{R}(\tau)]$ , see eqs. (19), (21). Hence we investigate this force correlation function.

First we consider the averaged quadratic force for  $\Delta\tau = 0$  along the trajectory  $\mathbf{R}(\tau)$  of the inclusion to see whether differences in the strength of the correlations occur. Then we will regard the dependence of the correlations on the time interval  $\Delta\tau$ . To examine the strength of the correlations for  $\Delta\tau = 0$  the quadratic force acting on the inclusion is determined at each time step of the simulation and then averaged over all values. For several sets of parameters we receive the values that are plotted in fig. 6 as a function of  $\sigma\beta\ell^2$  for a constant  $\kappa\beta$  and in fig. 7 as a function of  $\kappa\beta$  for a constant  $\sigma\beta\ell^2$ . The values resulting from the analytical calculations are also plotted in these figures. We observe a difference between analytical and simulation results that is on the same order of magnitude as the difference in the diffusion coefficients. In the analytical calculations we assume that the probability of finding the inclusion at a particular position is the same for any point of the membrane. If we calculate, using the simulation data, the mean square

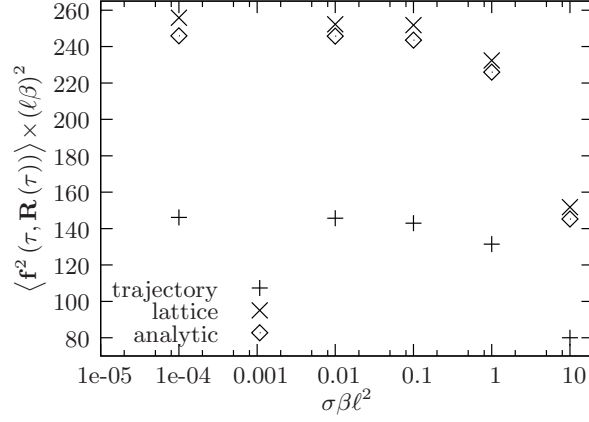


Figure 6: Average over the squared force on the inclusion for equal times  $\langle \mathbf{f}^2(\tau, \mathbf{R}(\tau)) \rangle$  as a function of the effective tension  $\sigma\beta\ell^2$  for the fixed bending rigidity  $\kappa\beta = 5$ . The figure shows a good agreement between the analytical points ( $\diamond$ ) and those achieved by averaging over a fixed point on the lattice (x). The averaging along the trajectory (+) leads to smaller values.

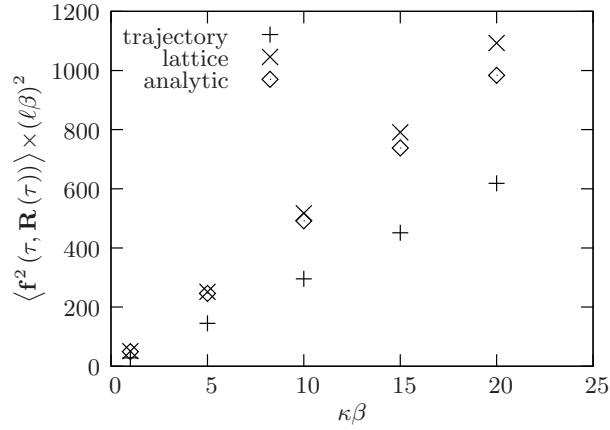


Figure 7: Average over the squared force on the inclusion for equal times  $\langle \mathbf{f}^2(\tau, \mathbf{R}(\tau)) \rangle$  as a function of the bending rigidity  $\kappa\beta$  for the fixed surface tension  $\sigma\beta\ell^2 = 0$ . The figure shows a good agreement between the analytical points ( $\diamond$ ) and those achieved by averaging over a fixed point on the lattice (x). The averaging along the trajectory (+) leads to smaller values.

of the force the inclusion would be exposed to if it were fixed at some arbitrary position on the membrane we obtain values very close to the mean squared force resulting from the analytical calculations. These values are also plotted in figs. 6 and 7. The differences in fig. 6 between the analytical calculations and the average for a fixed point are caused by the time step  $\Delta t$  of the simulations that induces bigger numerical errors for higher values of  $\kappa\beta$  as previously explained in section 5. Overall, averaging over the whole lattice in the calculations leads to seemingly higher forces than along the actual particle trajectory. A possible explanation for this reduced force is that most of the time the inclusion is close to a local minimum of the free energy. The extrema of the energy are created by the membrane shape, which is constantly changing due to thermal fluctuations. Therefore, the positions of the extrema will also move along the membrane. As the negative gradient of the energy is always pointing towards the nearest local minimum the inclusion will predominantly move in the direction of the nearest local minimum. For a fast enough diffusion rate the inclusion is capable of following a local minimum.

Due to the fact that for each simulation run a new thermally equilibrated membrane is used and the particle is always placed in the center of the membrane, it is very unlikely that the inclusion is initially close to an energy minimum. Therefore, the inclusion is exposed to higher forces at the beginning than at later times. Since higher forces go along with a higher diffusion rate we expect to observe two diffusion coefficients from the simulation data: a smaller one for late and a larger one for early times. Indeed such a behavior occurs as one can see in fig. 3 where the linear fits to the mean square displacement for early and late times are plotted. In this example the crossover is at about 0.2ms. Comparing the resulting diffusion coefficients with the analytical values, the one determined at the beginning of the simulation agrees reasonably well with the analytically determined diffusion coefficient. The inclusion starts with a higher diffusion rate and then, after a variable time period, finds a local minimum, which it tries to follow.

Now that we have found that the force acting on the inclusion is reduced in the simulations we consider the time correlations of the force  $\langle \mathbf{f}(\tau, \mathbf{R}(\tau)) \cdot \mathbf{f}(\tau + \Delta\tau, \mathbf{R}(\tau + \Delta\tau)) \rangle$ . We expect to see a reduction of the correlations caused by the inclusion following an energy minimum but in addition the time dependency will be influenced by the movement of the particle position  $\mathbf{R}(\tau)$ . The obtained correlation function along the trajectory is plotted in fig. 8 together with the analytical result for  $\kappa\beta = 5$  and vanishing tension. For a better representation the functions are normalised to one and plotted for small  $\Delta\tau$  in the inset of the figure. It is obvious that in addition to the altered start values the time dependence is also different. The decay of the correlations along the trajectory is slower than for the analytical curve. To demonstrate that this altered decay is caused by the motion of the inclusion we choose five fixed points of the lattice and determine, from the simulation data, the time correlation function of the force that would act on the inclusion if it were fixed at these points. The average over these points is also plotted in fig. 8 and agrees well with the analytical curve. The altered decay along the trajectory is an effect caused by the motion of the particle and indicates that the force correlations are stronger along the trajectory. This fact does not only lead to a slightly higher diffusion rate but also shows that the forces for a series of time steps point in similar directions which corroborates our interpretation that the inclusion tries to follow a local minimum. Although a larger decay time of correlations leads to enhanced diffusion the observed diffusion rate is smaller than the analytically calculated value since the effect that forces close to energy minima are reduced dominates.

## 8 Conclusions

In this paper, we have derived a model for the interaction of an inclusion with a model membrane and have investigated the influence of this interaction on the diffusion of the inclusion. In the model the inclusion is a physical object with an area, a spontaneous curvature and a bending rigidity. In analogy to Helfrich's free energy a new free energy is derived and with this coupled equations of motion for the inclusion and the membrane dynamics. Using these stochastic equations and employing several approximations we calculate the curvature-coupled diffusion coefficient  $D_{cc}$ . To assess the quality of the approximations in this analytical calculation that assumes a weak perturbation of the membrane we set up simulations. These simulations that numerically integrate the coupled equations of motion for the membrane and the inclusion are also based on the unperturbed membrane equation.

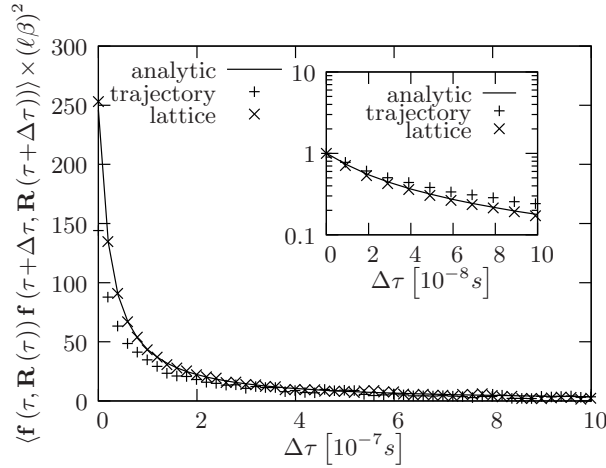


Figure 8: Time correlation function of the additional force on the inclusion  $\langle \mathbf{f}(\tau, \mathbf{R}(\tau)) \cdot \mathbf{f}(\tau + \Delta\tau, \mathbf{R}(\tau + \Delta\tau)) \rangle$  for the bending rigidity  $\kappa\beta = 5$  and the effective tension  $\sigma\beta\ell^2 = 0$  as a function of the time difference  $\Delta\tau$ . In the inset the first  $10^{-7}s$  of the time correlation function are plotted scaled to one for  $\Delta\tau = 0$ . A good agreement is found for the analytical curve (line) and the average over five fixed lattice points (x). The time dependence of the force correlations along the trajectory (+) is different from the analytical result.

Both, the simulations and our analytical approach, clearly display that the additional force on the inclusion caused by the interaction between particle and membrane leads to a significant increase in the diffusion coefficient compared to bare intramembrane diffusion. However, comparing the analytical calculations with the simulation results one finds that the curvature-coupled diffusion coefficient in the simulations is about 10% smaller than analytically expected, but follows the behavior qualitatively. A closer look at the forces on the inclusion shows that the averaged forces along the trajectory of the inclusion are smaller than the averaged notional forces acting at any arbitrary fixed point of the lattice. The average over the latter forces, however, has a good agreement with the values from the analytical calculations. Since smaller forces correspond to local extrema of the free energy, and the gradient, i.e. the force, always points to the nearest local minimum it is likely that the inclusion is in the vicinity of such a local minimum of the energy most of the time. If the mobility of the inclusion is big enough the inclusion is able to follow such a local minimum. Another point for this interpretation is that we place the inclusion in a new thermally equilibrated membrane for each simulation run. Hence, the inclusion is not necessarily close to a local minimum at the beginning and the diffusion rate should be faster for early times of the simulations. Considering the simulation data we find indeed that the diffusion for early times is about the same as the diffusion rate expected from the analytical calculation. After a short time the diffusion rate decreases and then remains constant. This corroborates the assumption that the inclusion meets a local minimum after some time and then tries to follow it.

Our study leads to the conclusion that the analytical calculations provide qualitative values for the curvature-coupled diffusion coefficient for a given set of parameters. For a quantitative value of the curvature-coupled diffusion coefficient simulations are necessary that take the effects of the movement of the inclusion into account.

In this paper we use the unperturbed membrane equation of motion. In ongoing work we are investigating the influence of the inclusion on the membrane dynamics and the diffusion by use of simulations that incorporate the perturbed membrane equation of motion. Then, the particle does not only adapt to the membrane but the membrane also adjusts to the particle. This will possibly lead to a further reduction of the diffusion coefficient compared to the analytical calculation. By comparing these results with those of the present paper it will be possible to determine the parameter range in which the perturbation may be neglected. We intend to also study the diffusion of several inclusions in a membrane in order to investigate possible cluster formation induced by membrane mediated interactions between the inclusions. Aside from this one may also be interested in other forms of interactions between the membrane and the inclusion

or additional interactions between the inclusions.

The investigation of several possible interactions and the resulting effects on the diffusion coefficient of inclusions as a function of membrane parameters may help to understand experimental data better and should finally lead to a deeper insight of the diffusion processes in biological membranes.

## References

1. Lippincott-Schwartz, J.; Snapp, E.; Kenworthy, A. *Nat. Rev. Mol. Cell Bio.* **2001**, *2*, 444-456.
2. Marguet, D.; Lenne, P. F.; Rigneault, H.; He, H.-T. *EMBO J.* **2006**, *25*, 3446-3457.
3. Lommerse, P. H. M.; Spaink, H. P.; Schmidt, T. *BBA-Biomembranes* **2004**, *1664*, 119-131.
4. Chen, Y.; Lagerholm, B. C.; Yang, B.; Jacobson, K. *Methods* **2006**, *39*, 147-153.
5. Reits, E. A. J.; Neefjes, J. J. *Nat. Cell Biol.* **2001**, *3*, E145-E147.
6. Lippincott-Schwartz, J.; Altan-Bonnet, N.; Patterson, G. H. *Nat. Cell Biol.* **2003**, *5*, S7-S14.
7. Kohl, T.; Schwille, P. *Adv. Biochem. Eng. Biot.* **2005**, *95*, 107-142.
8. Thompson, N. L.; Lieto, A. M.; Allen, N. W. *Curr. Opin. Struct. Biol.* **2002**, *12*, 634-641.
9. Saxton, M. *Annu. Rev. Biophys. Biomol. Struct.* **1997**, *26*, 373-399.
10. Kusumi, A.; Nakada, C.; Ritchie, K.; Murase, K.; Suzuki, K.; Murakoshi, H.; Kasai, R. S.; Kondo, J.; Fujiwara, T. *Annu. Rev. Biophys. Biomol. Struct.* **2005**, *34*, 351-378.
11. Tomishige, M.; Sako, Y.; Kusumi, A. *J. Cell Biol.* **1998**, *142*, 989-1000.
12. Edidin, M.; Kuo, S. C.; Sheetz, M. P. *Science* **1991**, *254*, 1379-1382.
13. Sbalzarini, I. F.; Hayer, A.; Helenius, A.; Koumoutsakos, P. *Biophys. J.* **2006**, *90*, 878-885.
14. Aizenbud, B. M.; Gershon, N. D. *Biophys. J.* **1982**, *38*, 287-293.
15. Holyst, R.; Plewczyński, D.; Aksimentiev, A. *Phys. Rev. E* **1999**, *60*, 302-307.
16. Plewczyński, D.; Holyst, R. *J. Chem. Phys.* **2000**, *113*, 9920-9929.
17. Faraudo, J. *J. Chem. Phys.* **2002**, *116*, 5831-5841.
18. King, M. R. *J. Theor. Biol.* **2007**, *227*, 323-326.
19. Yoshigaki, T. *Phys. Rev. E* **2007**, *75*, 041901.
20. Naji, A.; Brown, F. L. H. *J. Chem. Phys.* **2007**, *126*, 235103.
21. Brochard, F.; Lennon, J. F. *J. Phys. (Paris)* **1975**, *11*, 1035-1047.
22. Seifert, U. *Adv. in Phys.* **1997**, *46*, 13-137.
23. Gustafsson, S.; Halle, B. *J. Chem. Phys.* **1997**, *106*, 1880-1887.
24. Reister, E.; Seifert, U. *Europhys. Lett.* **2005**, *71*, 859-865.
25. Gov, N. S. *Phys. Rev. E* **2006**, *73*, 041918.
26. Reister-Gottfried, E.; Leitenberger, S.; Seifert, U. *Phys. Rev. E* **2007**, *75*, 011908.
27. Kahya, N.; Wiersma, D.; Poolman, B.; Hoekstra, D. *J. Biol. Chem.* **2002**, *277*, 39304-39311.
28. Vereb, G.; Szöllősi, J.; Matkó, J.; Nagy, P.; Farkas, T.; Vigh, L.; Mátyus, L.; Waldmann, T. A.; Damjanovich, S. *Proc. Natl. Acad. Sci. USA* **2003**, *100*, 8053-8058.
29. Forstner, M.; Yee, C.; Parikh, A.; Groves, J. *J. Am. Chem. Soc.* **2006**, *128*, 15221-15227.
30. Weikl, T. R.; Kozlov, M. M.; Helfrich, W. *Phys. Rev. E* **1998**, *57*, 6988-6995.
31. Weikl, T. R. *Europhys. Lett.* **2001**, *54*, 547-553.
32. Dommersnes, P. G.; Fournier, J.-B. *Eur. Phys. J. B* **1999**, *12*, 9-12.



33. Dommersnes, P. G.; Fournier, J.-B. *Eur. Phys. J. E* **2003**, *11*, 141-146.
34. Fošnarič, M.; Iglič, A.; May, S. *Phys. Rev. E* **2006**, *74*, 051503.
35. Cooke, I. R.; Deserno, M. *Biophys. J.* **2006**, *91*, 487-495.
36. Reynwar, B. J.; Illya, G.; Harmandaris, V. A.; Müller, M. M.; Kremer, K.; Deserno, M. *Nature* **2007**, *447*, 461-464.
37. Blood, P. D.; Voth, G. A. *Proc. Natl. Acad. Sci. USA* **2006**, *103*, 15068-15072.
38. Ayton, G. S.; Blood, P. D.; Voth, G. A. *Biophys. J.* **2007**, *92*, 3595-3602.
39. Helfrich, W. *Z. Naturforsch. C* **1973**, *28*, 693-703.
40. Safran, S. *Statistical Thermodynamics of Surfaces, Interfaces, and Membranes*; Addison-Wesley Publishing Company: Cambridge, 1994.
41. Risken, H. *The Fokker-Planck Equation*; Springer Verlag: Heidelberg, 2nd ed.; 1989.
42. Hänggi, P.; Thomas, H. *Phys. Rep.* **1982**, *88*, 207-319.
43. Frigo, M.; Johnson, S. G. "FFTW - for version 3.1.2", [www.fftw.org](http://www.fftw.org), 2006.